Section A-Research paper

Flower like $NiCo_2O_4$@$NiMoO_4$ Heterostructure Enabling Enhanced Electrochemical Performance for Supercapacitor Electrodes

A. Siveswari
Department of Physics, School of Basic Sciences, Vels Institute of Science Technology and Advanced Studies (VISTAS), Chennai -600117, India.
Email: meghabhasker@gmail.com
gowthamivijayakumar@gmail.com

Abstract

A novel electrode material of the three-dimensional (3D) multicomponent oxide of Nickel Cobaltite and Nickel Molybdate heterostructures ($NiCo_2O_4$@$NiMoO_4$) has been synthesized by a facile microwave irradiation method, and an X-ray diffractogram (XRD) measurement confirms the materials' crystalline phase. A surface composition analysis using XPS was conducted. $NiCo_2O_4$, $NiMoO_4$ and $NiCo_2O_4$@$NiMoO_4$ has a structure resembling a nanoplate, nanosheet, and coreshell, as demonstrated by HR-SEM and TEM investigation. For $NiCo_2O_4$, electrochemical tests revealed pseudocapacitive behavior. Among all $NiCo_2O_4$@$NiMoO_4$ displayed excellent supercapacitor performance with a high specific capacitance of 2724 F g^{-1} at 1 Ag^{-1} and high energy density of 83.5 Wh kg^{-1} with catalytic stability.

Keywords: Heterostructure, specific capacitance, supercapacitor, power density, energy density, microwave heating.

1. Introduction

Energy storage technologies with high performance, low cost, and environmental friendliness have received a lot of attention in recent years from both the industrial and academic worlds [1-3] due to the continuously growing demand for green energy. Researchers are investigating several electrode materials because supercapacitor components are more affordable and less dangerous. However, because to their low energy densities, for which battery-type electrodes are currently preferred, supercapacitors have a restricted range of practical applications. As electrode materials for supercapacitors, a variety of transition mono-/multi-metallic oxides or hydroxides have been studied [4,5]. The electrode materials used in supercapacitors can be divided into two groups based on the various energy storage processes: electric double-layer capacitors (EDLCS) and pseudo capacitors (PCS) [6]. In

comparison to EDLCs, PCS have significantly greater capacitance values and energy densities due to their rapid and reversible redox reaction [7].

The hydrothermal method is one of the more traditional ways to create different nanomaterials among the numerous synthesis procedures. It's interesting that several nanomaterials with varying dimensions, dopants, core-shell configurations, heterostructures, etc. have been discovered to be effective for energy storage applications [8,9]. Due to its high theoretical capacitance, low cost, abundance, and environmental friendliness, nickel-cobalt metal oxide has received a great deal of study attention. Additionally, it is anticipated to offer richer redox reactions than the two comparable single-component oxides, incorporating contributions from both nickel and cobalt oxides [10]. However, due to their low electrical conductivity and small surface area, transition metal oxides, such as $NiCo_2O_4$, typically exhibit restricted kinetics during the redox reaction [11]. Interestingly, metal molybdates as $NiMoO_4$ have a low rate performance despite having a high specific capacitance due to the strong electrochemical activity of nickel ions.

When compared to pure $NiCo_2O_4$, hetero-nanostructured $NiCo_2O_4$@$NiCo_2O_4$ and $NiCo_2O_4$@NiO at 0.5 A g^{-1} exhibit superior cycling stability, good rate capability, and high specific capacitance of 1925 and 2210 F g^{-1}, respectively. These materials exhibit excellent electrochemical performance [13]. The spinel nickel cobaltite ($NiCo_2O_4$), one of the ternary metal oxides (TMOs), has one of the highest theoretical specific capacitances, the best electrical conductivity, and the highest electrochemical activity [14]. The synthetic composite had a high specific capacitance of 2220Fg^{-1} at 1 A g^{-1} and demonstrated improved faradic behavior. Simple solvothermal synthesis produced a nickel foam supported NiO@$NiCo_2O_4$, with a significant specific capacitance of 1623.6 F g^{-1} at 2 A g^{-1}[15].

Jiang et al. created $NiMoO_4$ nanoclusters with one-dimensional nanorods using a simple microwave-assisted technique, and they demonstrated a capacitance of 680 F g^{-1} at 1 A g^{-1} [16]. According to Mai et al., the hierarchical-pore nanowires of heterostructured $MnMoO_4/CoMoO_4$ are superior to the mono-metal oxide of MnO_2 or Co_3O_4, having a specific capacitance of 187.1 F g^{-1} at a current density of 1 A g^{-1} and a cycling efficiency of 98% after 1,000 cycles [17]. However, due to the poor conductivities of pure $NiMoO_4$, which limit their practical applicability, the specific capacitances of $NiMoO_4$-related materials are significantly lower than their theoretical values. Due to their synergistic effects, an array of heterostructured materials demonstrated better electrochemical performance [18].

Microwave heating (MWH) is a synthesis technique that has the advantages of rapid heating and high reaction rates, as well as low energy consumption, high heating efficiency, and much shorter reaction times. As a result, the cost of finished products can be reduced [19,20]. Additional benefits of MWH include its excellent selectivity, homogenous volumetric heating, and high microwave penetration depth.

In the current work, a unique $NiCo_2O_4$@$NiMoO_4$ core-shell electrode material was created using the microwave oven approach. Since $NiMoO_4$ and $NiCo_2O_4$ are both promising candidate materials for supercapacitors on their own, the combination of the two materials to form a complex core-shell structure is anticipated to significantly increase the surface area to provide more electroactive sites for Faradaic reactions and create quick pathways for electrolytic ions and electron diffusion and transportation, as well as to enable synergistic

effects of $NiCo_2O_4$ and $NiMoO_4$ to increase the capacity of the super simple microwave irradiation significantly was used to create the heterostructures. In order to create the core-shell heterostructure, the $NiMoO_4$ nano species is deposited outside of the $NiCo_2O_4$ nanoparticles. As a result, a two-step strategy involving microwave synthesis and calcination was suggested. The "core" was made of $NiCo_2O_4$, and the "shell" was made of $NiMoO_4$.

2. Experimental Analysis

Nanomaterials of $NiCo_2O_4$@$NiMoO_4$ were synthesized by facile microwave irradiation method.

2.1 Synthesis of $NiC0_20_4$

For the synthesis of $NiCo_2O_4$, initially, nickel nitrate hexahydrate and cobalt nitrate hexahydrate were taken in 1:2 weight ratio and the precursors were dissolved in the mixture of distilled water and ethanol (40 ml: 40ml). A homogenous $Ni-Co$ precursor solution was obtained after the vigorous stirring for 30 min. The required amount of NaOH pellets were introduced to the above solution with continuous stirring for 30 min. The resultant solution was kept in the LG microwave oven (MH-4048 GW) to undergo microwave irradiation. The output power was maintained as 800 W with an operating frequency of 2.45 GHz. Theirradiation was continued for 5 min and then it was left to cool down to the ambient temperature. The obtained product was subjected to wash with double distilled water and ethanol to remove the ions and byproducts. In order to dry, the product was kept in a hot-air oven at 60°C for 12 h. The dried product was mixed well and kept in a muffle furnace for annealing at 400°C for 4 h. After annealing, dark green colour powder was obtained.

2.2 Synthesis of $NiCo_20_4$@$NiMo0_4$

The $NiMoO_4$ was grown on the prepared $NiCo_2O_4$ to form the $NiCo_2O_4$@$NiMoO_4$ material also by a microwave heating method. 0.25g of freshly prepared $NiCo_2O_4$ was added to 80 ml of Distilled water in a clean beaker. Now add 1.164 g of Nickel (II) Nitrate Hexa hydrate $Ni(NO_3)_2.6H_2O$ to the above solution and stir for 20-30 mts. Now add 0.823g of Sodium Molybdate Hepta Hydrate Na_2MoO_4. to the above solution again stir well for 20-30 min using a magnetic stirrer for obtaining a homogenous solution. The final solution was transferred into a clean thick glassed beaker kept in a household microwave oven (2.45 GHz) with power up to 1 kW and irradiated for 2,3,5 till 8 minutes in steps with the ON/OFF conditions to avoid overheating. After cooling down to room temperature, the products were taken out and rinsed with deionized water and ethanol for 2-3 times, then dried at 60°C for 3 h. Then the remaining synthesis procedure such as the microwave process, drying and annealing at 350^oC in air for 2 h were followed as similar to the procedure which was followed for the $NiCo_2O_4$ synthesis. Schematic representation of the synthesis process of $NiCo_2O_4$@$NiMoO_4$ is shown in Fig. 1.

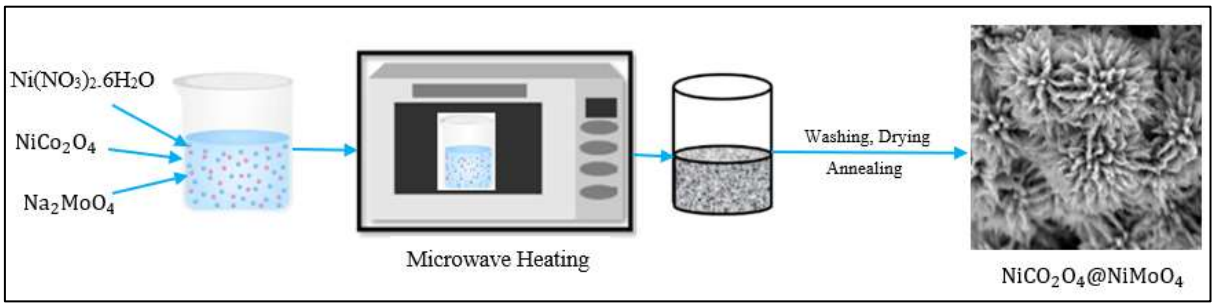

Fig.1. Synthesis scheme of $NiCo_2O_4$@$NiMoO_4$

2.3 Characterizations techniques

Powder X-ray diffraction (XRD) analysis was done using PANalytical, Netherlands, using $\mathrm{Cu} - K\alpha$ radiation in the 2θ range from 10^o to 80^o to evaluate the crystalline phase of the produced materials. X-ray photoelectron spectroscopy (XPS, PHI Versa probe III) with $\mathrm{Al}K\alpha$ monochromatic radiation analysis was used to evaluate the surface elemental compositions. The surface morphology and nanostructures of the prepared materials were photographed using a High-Resolution Scanning Electron Microscope (HR-SEM) and aHigh-Resolution Transmission Electron Microscope (HR-TEM) using Thermo scientific Apreo S, JEOL Japan and JEM-2100 Plus, respectively. The electrochemical performance was further explored using galvanostatic charge-discharge measurements.

2.4 Electrochemical measurements

The three-electrode system, which includes active material coated nickel foam, silver/silver chloride, and platinum wire as working electrodes, references, and counter electrodes, was used to study the electrochemical properties. To remove the electrode's surface particles, 2×1 cm of nickel foam was taken and sonicated with ethanol and acetone for a short period of time. In order to create the working electrode, first 85 wt.% of the active material, 10 wt.% of carbon black, and 5 wt.% of polyvinylidene fluoride (PVDF) were thoroughly mashed in a mortar pestle and made slurry by introducing few drops of N-Methyl-2-pyrrolidinonewith the above mixture. The resultant slurry was coated uniformly at 1×1 cm on a pre-treated Ni foam, and it was then dried at 60^oC for 24 hours. Using a Bio-Logic SP 300 (France) electrochemical workstation, the constructed electrodes were tested for electrochemical performance in a 1 M KOH electrolyte solution. The following equation is used to compute the specific capacitance:

$$C_s = \frac{I\Delta t}{m\Delta V}$$

where I (A) represents the discharge current, $C(\mathrm{Fg^{-1}})$ is the specific capacitance, and $m(\mathrm{mg}), \Delta V(\mathrm{V})$, and $\Delta t(\mathrm{s})$ designate the mass of active materials, potential drop during discharge, and total discharge time respectively.

3. Results and discussion

3.1 Formation mechanism of $NiCo_2O_4$@$NiMoO_4$ core-shell nanomaterials

The formation mechanism of $NiCo_2O_4$@ $NiMoO_4$ core-shell nanomaterials is proposed by facile microwave irradiation method. Nano-$NiCo_2O_4$ cores were first created. Then to create the final hierarchical $NiCo_2O_4$@$NiMoO_4$ core shell nanomaterials, a thin coating of NiMoO4 was deposited onto the surface of the $NiCo_2O_4$ cores.

3.2 XRD analysis

The XRD analysis was used to examine the crystal structures of $NiCo_2O_4$, $NiMoO_4$ and $NiCo_2O_4$@$NiMoO_4$ as they were produced. $NiCo_2O_4$@$NiMoO_4$ reaches its maximum peak at 1750 at intensity a.u. at 27.6 (2θ deg.) as shown in Fig. 2. The (111), (220), (311), (222), (400), (422), (511) and (440) crystal planes of $NiCo_2O_4$ can be indexed as the diffraction peaks at 19.2, 31.4,35.8, 36.8, 39.7, 46.3, 56.8, 60.4, 67.2° (JCPDS card no. 73-1702). The low crystallinity of the pure $NiCo_2O_4$ is indicated by the large diffraction peaks. The standard patterns for $NiMoO_4 \cdot xH_2O$ (JCPDS, card no. 13-0128) and the patterns of single $NiMoO_4$ are in remarkable accord. $NiMoO_4$ impurity phase was also linked to a number of diffraction peaks (JCPDS, card no. 12-0348). The pattern of $NiCo_2O_4$@$NiMoO_4$ contains the peaks of $NiCo_2O_4$@$NiMoO_4$ (JCPDS, card no.12-0348), and $NiMoO_4 \cdot xH_2O$ (JCPDS, card no.13-0128), showing that two phases of as-synthesized $NiMoO_4$ are coexisting on the surface of $NiCo_2O_4$. Because $NiMoO_4$ nanosheets wrap around the surface of the $NiCo_2O_4$ nanostructure and cover $NiCo_2O_4$ with strong diffraction peaks, the intensity of the diffraction peaks corresponding to $NiCo_2O_4$ is reduced in the patterns of $NiCo_2O_4$@$NiMoO_4$ materials.

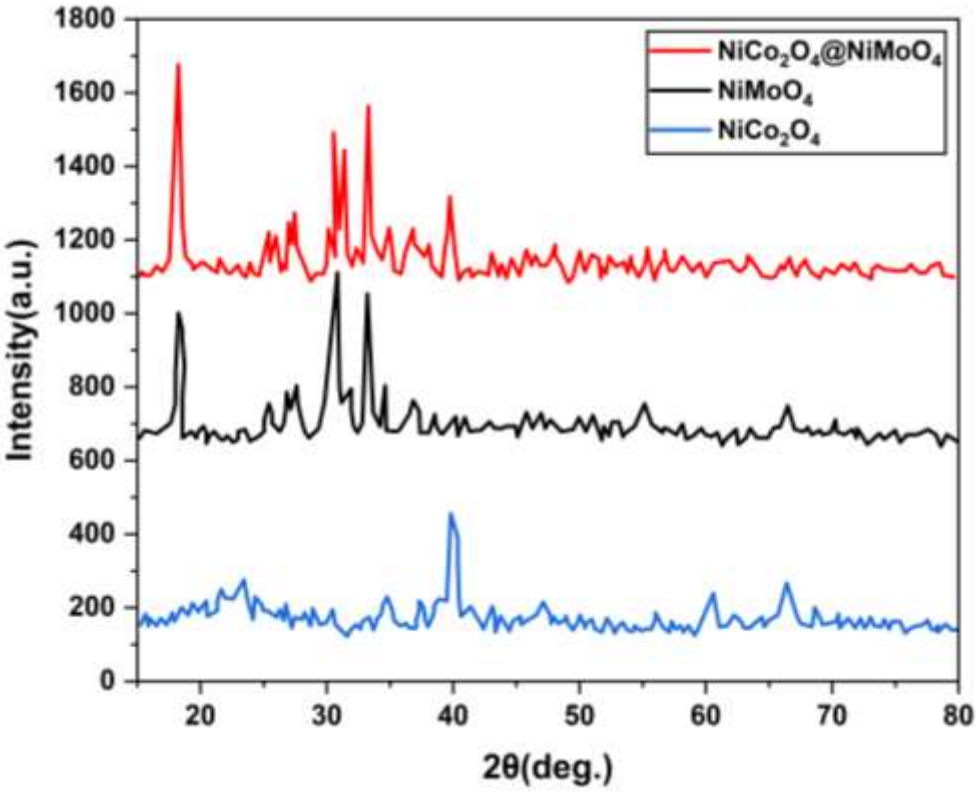

Fig. 2. XRD patterns of $NiCo_2O_4$@$NiMoO_4$

3.3 XPS analysis

The elemental composition and oxidation state of $NiCo_2O_4$@$NiMoO_4$ as synthesized are further understood by XPS measurements, which show the presence of Ni, Mo, Co, and O as well as C from the reference and the absence of any other element. The $Ni2p_{3/2}$ level is represented by the binding energy peak at 857.4eV and its satellite peak at 864.8eV, whereas the $Ni2p_{1/2}$ level is represented by the binding energy peak at 881.7eV and its satellite peak at 887.3 eV as depicted in Fig. 3(a). $Ni2p_{3/2}$ and $Ni2p_{1/2}$ have major binding energy peaks that are 17.8eV apart from one another, which is a characteristic of the Ni^{2+} oxidation state. The Mo 3d core level spectra (Fig. 3(b)) display two peaks for Mo 3d5/2 and Mo 3d3/2, respectively, with binding energies of 232.8 eV and 236.9 eV. Mo 3d has binding energy peaks that are 3.1 eV apart, which also denotes a Mo(VI) oxidation state.

More specifically, Co^{2+} is responsible for the fitting peaks at 783.4 eV and 797.5eV, the binding energies (EB) of Co(II) ions, whereas Co^{3+} and two shake-up satellites (referred to as "Sat.") are responsible for the fitting peaks at 784.9 and 798.2 eV, as illustrated in Fig. 3(c). Three contributions from oxygen are visible in the high-resolution spectra of the O1s area. The peak at 530.2eV in particular, is typical of metal-oxygen bonding. The peak at 531.4eV is frequently linked to flaws, impurities, and various surface species, such as hydroxyls, chemisorbed oxygen, under-coordinated lattice oxygen, or species native to the spinel's surface.

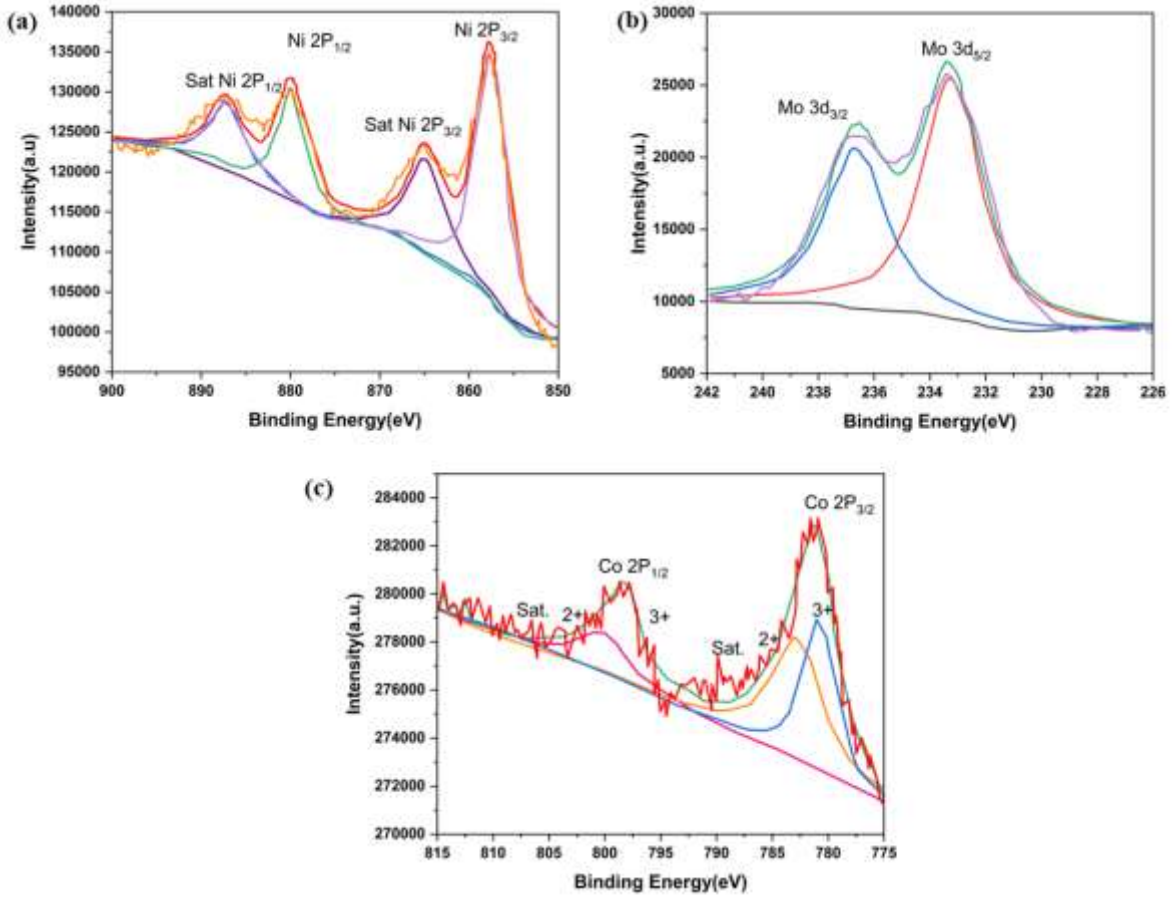

Fig. 3. XPS spectra (a)Ni 2p, (b) Co 2p and (c) Mo 3d for flower like $NiCo_2O_4$@$NiMoO_4$ microspheres

The plurality of physi- and chemisorbed water at or near the surface is the probable cause of the peaks at 532.6eV. These findings demonstrate that Ni^{2+}, Ni^{3+}, Mo(vr), Co^{2+}, Co^{3+} and O^{2-}, are present in the surface composition of the as-synthesised $NiCo_2O_4$@$NiMoO_4$ material, which is in good accord with the findings of $NiMoO_4$ and $NiCo_2O_4$ as core-shell structure: The "core" was made of $NiCo_2O_4$, and the "shell" was made of $NiMoO_4$. It is obvious that it is made up of Ni, Co, Mo, and O elements. The parent hierarchical heterostructures are a mixture of $NiCo_2O_4$ and $NiMoO_4$, which is in good agreement with the XRD data, and the nanosheets that have formed on the surface are primarily made up of $NiMoO_4$.

3.4 Morphological analysis

The morphologies of $NiCo_2O_4$ and $NiCo_2O_4$@$NiMoO_4$ were studied by FESEM, as illustrated in Fig. 4. As seen in Fig. 4(a) the $NiCo_2O_4$ material possesses a flower-like characteristic with a 5μm diameter and sharp nano-needles. Fig 4(b) displays the SEM image of $NiMoO_4$.

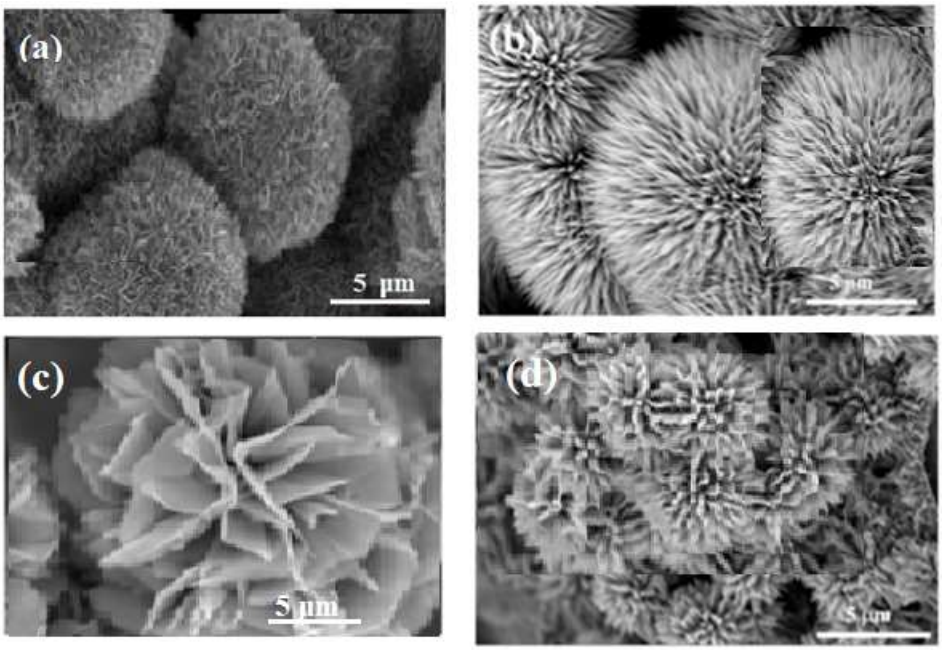

Fig. 4. (a) SEM image of the $NiCo_2O_4$; (b) SEM image of $NiMoO_4$; (c, d) SEM images of core–shell $NiCo_2O_4$@$NiMoO_4$ nanostructures.

The SEM image of the $NiCO_2O_4$@$NiMoO_4$ core-shell material is shown in Fig. 4(c) and (d). However, the needles of $NiCo_2O_4$ were uniformly wrapped by short $NiMoO_4$ nanorods to form a core-shell nanostructure, resulting in $NiCo_2O_4$@$NiMoO_4$ bristled nanorods of about 200 nm diameter. It is clear that the fundamental structure of $NiCo_2O_4$ is still preserved. The

coated nanorods outside of the $NiCo_2O_4$ needles also have a flower-like morphology, as seen in Fig. 4(d).

TEM and HRTEM are used to examine the morphology and structure of the $NiCo_2O_4$ and $NiCo_2O_4$@$NiMoO_4$ core-shell nanomaterial in greater detail.

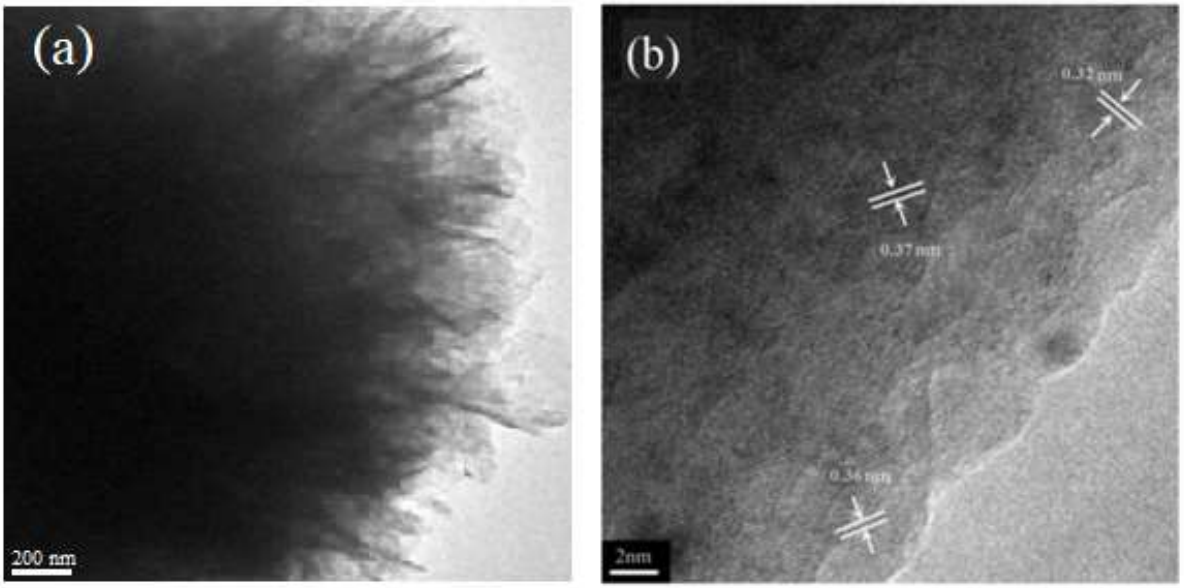

Fig. 5. (a) Low-magnification TEM image, (b) HRTEM image of the NiCo2O4@NiMoO4 core–shell nanostructures

According to Fig. 5(a), $NiCo_2O_4$ exhibits flower-like shape with pointed nanoneedles that radiate from the center of the ball. It is extremely compatible with FESEM findings. The high-resolution TEM (HRTEM) image reveals that the $NiCo_2O_4$ (311) crystal plane's lattice spacing is 0.36 nm. Unfortunately, $NiMoO_4$'s crystal structure is not well understood, therefore it is still unclear to which plane the measured gap belongs. The diameter of the nanorods $NiCo_2O_4$@$NiMoO_4$ (the edge of the dark image) is around 200 nm, which is in good agreement with that of SEM. Fig. 5(b) shows the HRTEM image of the $NiMoO_4$ shell. The lattice spacing of 0.32 nm is similar to that of 0.319 nm in the JCPDS 13-0128 file, while the interplanar spacings are 0.36 nm and 0.37 nm, respectively, which are comparable to the values of 0.365 nm and 0.37 nm provided in the JCPDS 12-0348 file. The $NiCo_2O_4$@$NiMoO_4$ material's high porosity and expansive surface are attributable to the hierarchical mesopores that are formed when $NiMoO_4$ nanorods assemble and aggregate on the $NiCo_2O_4$ needles.

3.5 Electrochemical measurements

Pure $NiCo_2O_4$ > $NiMoO_4$ is followed by $NiCo_2O_4$@$NiMoO_4$ in terms of integral CV area and height of oxidation peak, showing that the former electrode has a higher specific capacitance than the latter two. The increased electrochemical reaction activity of the core-shell nanoflake arrays may be attributed to the $NiMoO_4$ shell's enhanced contribution to the pseudocapacitance. As synthesized $NiCo_2O_4$@$NiMoO_4$ nanomaterials may be used in electrochemical supercapacitors because of their porous architectures and large surface areas,

which may help with ion transfer at the electrode/electrolyte interface. The area of the $NiCo_2O_4$@$NiMoO_4$ electrode, in contrast to that of $NiMoO_4$, exhibits a clear rise on the left side of the redox peaks. $NiCo_2O_4$ is the primary cause of this expanded area. This suggests that $NiCo_2O_4$@$NiMoO_4$ electrode materials perform better in supercapacitive applications when both $NiMoO_4$ and $NiCo_2O_4$ are present.

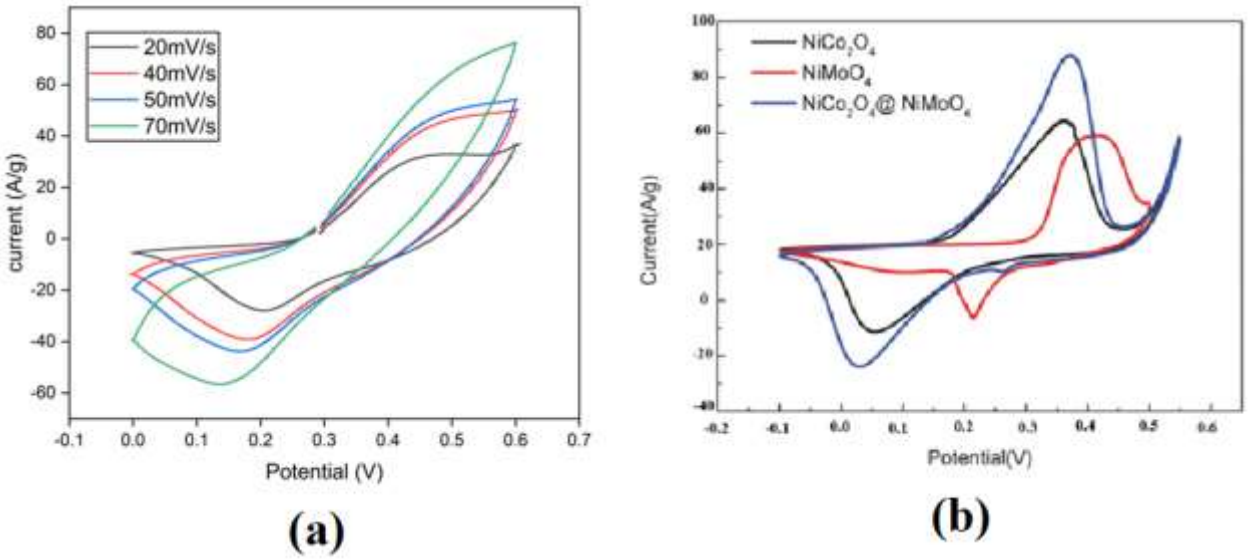

Fig. 6 Electrochemical performances of $NiCo_2O_4$, $NiMoO_4$ and $NiCo_2O_4$@$NiMoO_4$ (a) CV curves at different scan rates for $NiCo_2O_4$@$NiMoO_4$ electrode; (b) comparative CV curves.

The $NiCo_2O_4$@$NiMoO_4$ electrode's CV curves are displayed in Fig. 6(a) at scan rates of 20, 40, 50, 70 mVs^{-1} in the potential range of 0.0 to 0.6 V (vs. SCE). It is clear that the peak current increases as the scan rate rises, indicating that at the provided scan rates, the interfacial kinetics and rates of electronic and ionic transport are fast enough. The polarization action of the electrode is responsible for the anodic peaks shifting towards the positive potential and the cathodic peaks shifting towards the negative potential. The cyclic voltammetry (CV) curves of the $NiCo_2O_4$, $NiMoO_4$, and $NiCo_2O_4$@$NiMoO_4$ electrodes are shown in Fig. 6(b) at a scan rate of 10mVs^{-1}. The three electrodes clearly show a pair of redox peaks, specifically oxidation peaks at 0.35, 0.40, 0.36 V and reduction peaks at 0.04, 0.22, 0.03 V for $NiCo_2O_4$, $NiMoO_4$ and $NiCo_2O_4$@$NiMoO_4$, respectively. These peaks are primarily attributed to the redox reactions of the Ni and Co species in the alkaline electrolyte.

During the procedure, a clear plateau region may be seen, pointing to the electrodes' pseudocapacitive activity. Fig. 7(a) displays the computed specific capacitances for the three electrodes at varying discharge current densities. The specific capacitance of $NiCo_2O_4$@$NiMoO_4$(2724 Fg^{-1}) is significantly higher than that of pure $NiCo_2O_4$(1685 Fg^{-1}) and $NiMoO_4$(1435 Fg^{-1}) at a current density of 1 Ag^{-1}. Even though there is insufficient active material involved in the redox reaction at high current densities and the specific capacitance gradually decreases with increasing current density due to the incremental voltage drop, the specific capacitance is still as high as 2428 Fg^{-1} as the current

density increases 20 times, from 1 to 20 Ag^{-1} indicating that the $NiCo_2O_4$@$NiMoO_4$ electrode has a super high rate charge-discharge performance.

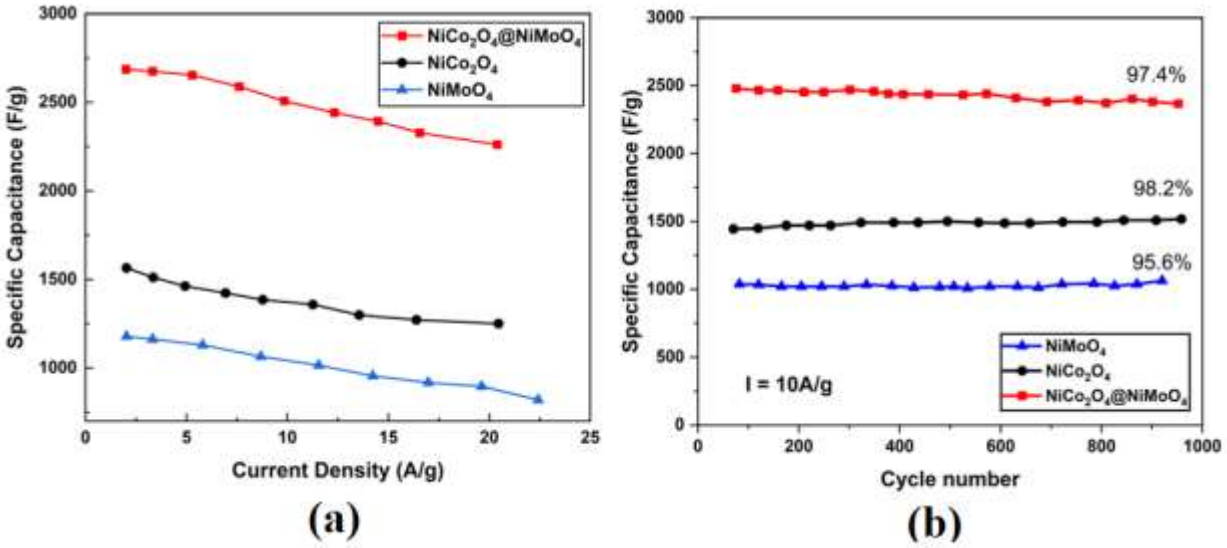

Fig. 7. (a) Specific capacitance as a function of discharge current density; (b) variation of specific capacitance with cycle numbers at a current density of 10 Ag^{-1}**.**

At 10 Ag^{-1}, the cycle stabilities of the $NiCo_2O_4$, $NiMoO_4$ and $NiCo_2O_4$@$NiMoO_4$ electrodes were measured and the results are presented in Fig. 7(b). It is evident that after 1000 cycles at 10 Ag^{-1}, the $NiCo_2O_4$ and $NiMoO_4$ exhibit specific capacitances of 1064 Fg^{-1} and 1492 Fg^{-1} and capacitance retention of 95.6% and 98.2%, respectively. The $NiCo_2O_4$@$NiMoO_4$ hybrid electrode has a very high specific capacitance of 2356 Fg^{-1} after 1000 cycles in addition to having a strong capacitance retention of 97.4%.

It is noteworthy that the specific capacitance of the $NiCo_2O_4$@$NiMoO_4$ electrode used in this research is also higher than that of other core-shell nano architectured materials that have been previously described, as shown in Table 1.

Table 1. Comparison of core-shell nanoarchitecture materials

Reference	**Nanomaterials**	**Method**	**Specific Capacitance** Fg^{-1} at 1 Ag^{-1})
[21]	$NiCo_2O_4$@$NiCo_2O_4$	Hydro	1917
[21]	$NiCo_2O_4$@NiO	Hydro	2105
[22]	$NiCo_2O_4$@graphene	Hydro	778
[23]	Co – NiO core-shell	Hydro	956
[24]	$NiCo_2O_4$@ $NiMoO_4$	Hydro	2474
Proposed method	$NiCo_2O_4$ @ $NiMoO_4$	Microwave	**2724**

The hierarchical $NiCo_2O_4$@$NiMoO_4$ electrode and the EIS of $NiCo_2O_4$, $NiMoO_4$, are displayed in Fig. 8(a). The semicircle is clearly visible in the inset and occurs frequently. All of the impedance spectra are comparable, consisting of a high-frequency semicircle followed by a low-frequency linear component. The two curves differ in two ways. First, the internal resistances (R_b) in the high frequency intercept of the real axis were different. The R_b of $NiCo_2O_4$@$NiMoO_4$ electrode reduced when compared to $NiMoO_4$, indicating that the addition of $NiCo_2O_4$ enhanced the electrode's ability to conduct electrons. Second, the diffusive resistance (Warburg impedance) of the $NiCo_2O_4$@$NiMoO_4$ electrode was lower than that of $NiMoO_4$, as shown by the straight line at low frequency. This finding suggests that the porous structure of the $NiCo_2O_4$@$NiMoO_4$ composite can lower the mass-transfer resistance and enhance the penetration of the electrolyte as well as ion diffusion in the host material. A minor pseudo charge transfer resistance (R_{ct}), which corresponds to the minimal semicircle in the impedance plots, is also present in the $NiCo_2O_4$@$NiMoO_4$ electrode. The outstanding electrochemical capacitive characteristics of these binary metal oxide based composite materials are demonstrated by the low R_b, R_{ct}, and Warburg impedance values.

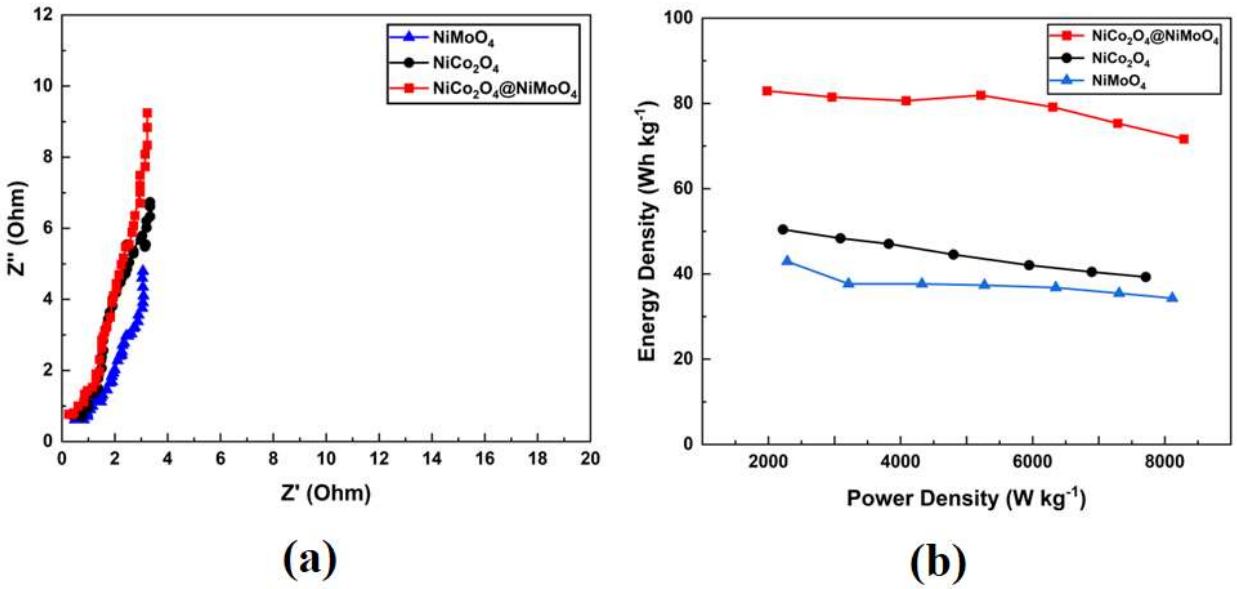

Fig. 8. (a) AC impedance plots of three electrodes; (b) Ragone plot of the estimated specific energy and specific power at various charge–discharge rates.

We further compute the specific energy and power densities, which are the two crucial elements for the practical applications of electrochemical supercapacitors, in light of the high capacitance and great rate capability. Based on the following equations, one may get the specific energy density (E) and power density (P), respectively:

$$E = \frac{1}{2} C \Delta V^2$$

$$P = \frac{E}{\Delta t}$$

where C refers to the specific capacitance, E is the specific energy density, P represents the power density, ΔV is the voltage range and Δt is the discharge time. In Fig. 8(b), the data are displayed as Ragone plots. The $NiCo_2O_4$@$NiMoO_4$ sample has the ability to produce high power outputs between 1485 and 8294 Wkg^{-1}, with little loss of high energy density (between 83.5 to 79.2 Wh kg^{-1}). The other two samples, however, show similar power densities with slightly lower but still striking energy densities. The current mesoporous $NiCo_2O_4$@$NiMoO_4$ hierarchical structures are very desirable as electrode materials for enhanced supercapacitors due to their remarkable ability to offer high specific power and energy densities.

According to the findings, the $NiCo_2O_4$@$NiMoO_4$ coreshell nanomaterial electrode has remarkable electrochemical performance as evidenced by its exceptionally high specific capacitance, low resistance, high cycle stability and capacitance retention, and good rate capability. All of these advantages are crucial for the real-world use in supercapacitors.

4. Conclusion

In this study, heterostructures of pure $NiCo_2O_4$ and $NiCo_2O_4$@$NiMoO_4$ were synthesized using a simple microwave irradiation approach, and their structural, morphological, and electrochemical analyses were conducted. The cubic crystal structure of the $NiCo_2O_4$@$NiMoO_4$ heterostructure was discovered using structural XRD measurements. By using HR-SEM and TEM to analyze the surface's morphology, the nanoplate-like structure of $NiCo_2O_4$@$NiMoO_4$ was observed. All prepared materials' elemental compositions and oxidation states underwent XPS analysis. The enhanced electro-chemical performance demonstrates that the inclusion of two metal oxides into a multifaceted core-shell hybrid nanostructure aligned with the electrically charged plates considerably increases the areal capacitance. The $NiCo_2O_4$@$NiMoO_4$ heterostructure demonstrated excellent supercapacitor performance with a high specific capacitance of 2724 F g^{-1} at 1 A g^{-1} and a high energy density of 83.5 Wh kg^{-1} at a power density of 1485 W kg^{-1}. This is according to electrochemical investigations on the synthesized materials in 1M KOH electrolyte. High recycling stability is also indicated by the device's high capacitance retention of 97.4 % after 1000 cycles of charge-discharge. As a result, the electrochemical research points to the $NiCo_2O_4$@$NiMoO_4$ heterostructure as a potential electrode material for supercapacitors' high-performance energy storage. The results show that any $NiCo_2O_4$@$XMoO_4$ core-shell electrode material has a high potential for use in electrochemical energy storage for supercapacitors employing microwave heating.

References

[1] Kong, D., Ren, W., Cheng, C., Wang, Y., Huang, Z., & Yang, H. Y. (2015). Three-dimensional $NiCo_2O_4$@ polypyrrole coaxial nanowire arrays on carbon textiles for high-performance flexible asymmetric solid-state supercapacitor. *ACS applied materials & interfaces*, *7*(38), 21334-21346.

[2] Nayak, A. K., Das, A. K., & Pradhan, D. (2017). High performance solid-state asymmetric supercapacitor using green synthesized graphene–WO3 nanowires nanocomposite. *ACS Sustainable Chemistry & Engineering*, *5*(11), 10128-10138.

[3] Nayak, A. K., & Pradhan, D. (2018). Microwave-assisted greener synthesis of defect-rich tungsten oxide nanowires with enhanced photocatalytic and photoelectrochemical performance. *The Journal of Physical Chemistry C*, *122*(6), 3183-3193.

[4] Mun, C. H., Gopi, C. V. M., Vinodh, R., Sambasivam, S., Obaidat, I. M., & Kim, H. J. (2019). Microflower-like nickel sulfide-lead sulfide hierarchical composites as binder-free electrodes for high-performance supercapacitors. *Journal of Energy Storage*, *26*, 100925. [CrossRef]

[5] Das, H. T., Mahendraprabhu, K., Maiyalagan, T., & Elumalai, P. (2017). Performance of solid-state hybrid energy-storage device using reduced graphene-oxide anchored sol-gel derived Ni/NiO nanocomposite. *Scientific reports*, *7*(1), 1-14. [CrossRef] [PubMed]

[6] Gai, Y., Shang, Y., Gong, L., Su, L., Hao, L., Dong, F., & Li, J. (2017). A self-template synthesis of porous $ZnCO_2O_4$ microspheres for high-performance quasi-solid-state asymmetric supercapacitors. *RSC advances*, *7*(2), 1038-1044. https://doi.org/10.1039/C6RA25950B

[7] Salunkhe, R. R., Kaneti, Y. V., & Yamauchi, Y. (2017). Metal–organic framework-derived nanoporous metal oxides toward supercapacitor applications: progress and prospects. *ACS nano*, *11*(6), 5293-5308. https://doi.org/10.1021/acsnano.7b0279 6

[8] Yedluri, A. K., & Kim, H. J. (2018). Wearable super-high specific performance supercapacitors using a honeycomb with folded silk-like composite of $NiCo_2O_4$ nanoplates decorated with $NiMoO_4$ honeycombs on nickel foam. *Dalton Transactions*, *47*(43), 15545-15554. [CrossRef]

[9] Yedluri, A. K., Anitha, T., & Kim, H. J. (2019). Fabrication of Hierarchical NiMoO4/NiMoO4 Nanoflowers on Highly Conductive Flexible Nickel Foam Substrate as a Capacitive Electrode Material for Supercapacitors with Enhanced Electrochemical Performance. *Energies*, *12*(6), 1143. [CrossRef]

[10] Tarasevich, M. R., Efremov, B. N., & Trasatti, S. (1982). Electrodes of conductive metallic oxides, part A. *Elsevier, USA*, 227.

[11] Liu, X. Y., Shi, S. J., Xiong, Q. Q., Li, L., Zhang, Y. J., Tang, H., Gu, C. D., Wang, X. L. and Tu, J. P. (2013). ACS Appl. Mater. Inter., 5, 8790–8795.

[12] Liu, M. C., Kong, L. B., Lu, C., Ma, X. J., Li, X. M., Luo, Y. C., & Kang, L. (2013). Design and synthesis of $CoMoO_4$–$NiMoO_4 \cdot xH_2O$ bundles with improved electrochemical properties for supercapacitors. *Journal of Materials Chemistry A*, *1*(4), 1380-1387.

[13] Zhou, W., Kong, D., Jia, X., Ding, C., Cheng, C., & Wen, G. (2014). $NiCo_2O_4$ nanosheet supported hierarchical core–shell arrays for high-performance supercapacitors. *Journal of Materials Chemistry A*, *2*(18), 6310-6315.

[14] Liu, S., Wu, J., Zhou, J., Fang, G. and Liang, S. (2015). Mesoporous $NiCO_2O_4$ nanoneedles grown on three dimensional graphene networks as binder-free electrode for high-performance lithium-ion batteries and supercapacitors, *Electrochim. Acta*, 176, 1-9. https://doi.org/10.1016/j.electacta.2015. 06.131

[15] Yao, D., Ouyang, Y., Jiao, X., Ye, H., Lei, W., Xia, X. & Hao, Q. (2018). Hierarchical NiO@$NiCo_2O_4$ core–shell nanosheet arrays on Ni foam for high-

performance electrochemical supercapacitors. *Industrial & Engineering Chemistry Research*, *57*(18), 6246-6256. https://doi.org/10.1021/acs.iecr.8b0046 7

[16] Wan, H., Jiang, J., Ji, X., Miao, L., Zhang, L., Xu, K., Chen, H. and Ruan, Y. (2013). Rapid microwave-assisted synthesis $NiMoO_4$ center dot H_2O nanoclusters for supercapacitors, Mater. Lett. 108, 164-167.

[17] Mai, L. Q., Yang, F., Zhao, Y. L., Xu, X., Xu, L., & Luo, Y. Z. (2011). Hierarchical $MnMoO_4$/$CoMoO_4$ heterostructured nanowires with enhanced supercapacitor performance. *Nature communications*, *2*(1), 381.

[18] Liu, J., Jiang, J., Cheng, C., Li, H., Zhang, J., Gong, H., & Fan, H. J. (2011). Co_3O_4 nanowire@ MnO_2 ultrathin nanosheet core/shell arrays: a new class of high-performance pseudocapacitive materials. *Advanced Materials*, *23*(18), 2076-2081.

[19] Bo, X., Xiang, K., Zhang, Y., Shen, Y., Chen, S., Wang, Y. & Guo, X. (2019). Microwave-assisted conversion of biomass wastes to pseudocapacitive mesoporous carbon for high-performance supercapacitor. *Journal of energy chemistry*, *39*, 1-7.

[20] Liang, J., Qu, T., Kun, X., Zhang, Y., Chen, S., Cao, Y. C., & Guo, X. (2018). Microwave assisted synthesis of camellia oleifera shell-derived porous carbon with rich oxygen functionalities and superior supercapacitor performance. *Applied Surface Science*, *436*, 934-940.

[21] Zhou, W., Kong, D., Jia, X., Ding, C., Cheng, C., & Wen, G. (2014). $NiCo_2O_4$ nanosheet supported hierarchical core–shell arrays for high-performance supercapacitors. *Journal of Materials Chemistry A*, *2*(18), 6310-6315.

[22] Wei, Y., Chen, S., Su, D., Sun, B., Zhu, J., & Wang, G. (2014). 3D mesoporous hybrid $NiCo_2O_4$@graphene nanoarchitectures as electrode materials for supercapacitors with enhanced performances. *Journal of Materials Chemistry A*, *2*(21), 8103-8109.

[23] Pan, G. X., Xia, X. H., Cao, F., Tang, P. S., & Chen, H. F. (2013). Fabrication of porous Co/NiO core/shell nanowire arrays for electrochemical capacitor application. *Electrochemistry communications*, *34*, 146-149.

[24] Zhang, Q., Deng, Y., Hu, Z., Liu, Y., Yao, M., & Liu, P. (2014). Seaurchin-like hierarchical $NiCo_2O_4$@ $NiMoO_4$ core–shell nanomaterials for high performance supercapacitors. *Physical Chemistry Chemical Physics*, *16*(42), 23451-23460.